Effect of Gate Electrode Work-Function on Source Charge Injection in Electrolyte-Gated Organic Field-Effect Transistors

Simone Fabiano, Slawomir Braun, Mats Fahlman, Xavier Crispin, and Magnus Berggren*

Systematic investigation of the contact resistance in electrolyte-gated organic field-effect transistors (OFETs) demonstrates a dependence of source charge injection versus gate electrode work function. This analysis reveals contact-limitations at the source metal-semiconductor interface and shows that the contact resistance increases as low work function metals are used as the gate electrode. These findings are attributed to the establishment of a built-in potential that is high enough to prevent the Fermi-level pinning at the metal-organic interface. This results in an unfavorable energetic alignment of the source electrode with the valence band of the organic semiconductor. Since the operating voltage in the electrolyte-gated devices is on the same order as the variation of the work functions, it is possible to tune the contact resistance over more than one order of magnitude by varying the gate metal.

1. Introduction

Organic field-effect transistors (OFETs) based on solution-processed semiconducting materials have undergone tremendous progress in recent years, primarily driven by the need for a low-cost electronics platform.[1] These progresses relate to both overall device performance and also reliability, which together show promise for practical applications based on OFET devices.[2] However, there are still both physical and technological issues to be faced before this technology can enter true applications. Contact resistance at the source electrode represents, for instance, one significant bottleneck to the transistor performance. Controlling the charge injection from metal electrodes into the organic semiconductor is one of the major hurdles to achieve scaling and size reduction of OFETs.[3] In an OFET, the electronic structure of the metal-semiconductor interface can strongly affect the overall device performance. Typically, charge injection into the device is efficiently achieved via an Ohmic contact, established at the source electrode, by choosing a metal with a work function that matches the highest occupied molecular orbital (HOMO) or lowest unoccupied molecular orbital (LUMO) of the organic semiconductor within a few tenths of an electronvolt.[4] Several interface modification methods have been reported to improve charge injection, such as interfacial dipole formation,[5] bulk doping of the organic semiconductor[6,7] or at the metal-organic interfaces.[8] In addition, with self-assembled molecular layers, expressing an intrinsic electric dipole moment at the interface, the work function of metal electrodes can be lowered or raised, thus affecting the magnitude of the charge injection.[9] This can be achieved, for example, by depositing a thiol-based self-assembled monolayer on the metal surface prior to the deposition of the organic semiconductor.[10]

Understanding the microscopic processes limiting the charge injection in OFETs is crucial to improve the performance of the OFETs. To this end, OFETs based on electrolyte insulators have a considerable potential due to their extraordinary high gate capacitance value, which allows device and circuit operation at extremely low voltages (typically less than 1 V). In fact, under an applied gate voltage, the ions of the electrolyte insulator drift to the active interface of the semiconductor and the gate metal, respectively, and establish two electric double layers across which the entire gate potential drops.[11] The charged sheets composing the electric double layers are separated by only a few Angstroms within the Helmholtz layer, leading to extraordinary high transversal electric fields (10^9 V m^{-1}).[12] Thus, the possibility to modulate the drain current with drive voltages of less then 1 V reveals new insight into phenomena that are not feasible with conventional inorganic or polymeric dielectric-based devices. Recently, we demonstrated for example that the threshold voltage measured in polyelectrolyte-gated OFETs is strongly dependent on the work function of the gate electrode and can be tuned by using different gate metals of different work function.[13]

Here, we demonstrate for the first time the dependence of charge injection on the gate electrode work function by systematically investigating the contact resistance in electrolyte-gated OFETs. Our analysis reveals contact-limitations at the metal-semiconductor interface, and shows that the contact resistance increases when low work function metals are used as the

Dr. S. Fabiano, Prof. X. Crispin, Prof. M. Berggren
Organic Electronics
Department of Science and Technology
Linköping University
SE-601 74, Norrköping, Sweden
E-mail: simone.fabiano@liu.se
Dr. S. Braun, Prof. M. Fahlman
Department of Physics
Chemistry and Biology
Linköping University
SE-581 83, Linköping, Sweden

DOI: 10.1002/adfm.201302070

gate electrode. Since the operating voltage in these devices is on the same order of magnitude as the variation of the work function between the gate electrode materials we find that it is possible to tune the contact resistance over more than one order of magnitude. The possibility to control the charge injection by changing the gate electrode is typically not feasible with conventional inorganic or polymeric dielectric gate insulators since the gate and drain-source driving voltages are relatively much higher in traditional OFETs. This supports the suitability of solid polyelectrolytes as dielectric layers in low voltage-operating devices optimized for circuit applications. Our approach would be of technological interest for further optimization of the device performance as well as for fundamental studies of transistor device physics.

2. Results and Discussion

Top gate, bottom contact transistors based on regioregular poly(3-hexylthiophene) (P3HT) were fabricated using poly(vinylphosphonic acid-*co*-acrylic acid) (P(VPA-AA)) as the electrolyte insulator (**Figure 1**a). The use of polyanions prevents anions penetration into the conjugated polymer and thus avoids electrochemical doping of the bulk semiconducting polymer layer (Figure 1b). This will guarantee that the electrolyte-gated OFET (EGOFET) runs entirely in the field-effect mode of operation. Figure 1c shows the output characteristics of four sets of P3HT-based electrolyte-gated OFETs with L = 50 μm (W = 1000 μm) at a fixed gate voltage and demonstrates the effect of different top-gate metals (i.e., Al, Ti, Cu and Ni) on the charge injection. Note that the gate voltage has been corrected for the transistor threshold voltage (V_{th}), taking into account the dependence of V_{th} on the work function of the gate electrodes.[13] Remarkably, the results show that Al reduces the drain current both in the linear and saturation regimes by nearly one order of magnitude as compared to the EGOFET including a Ni top-gate electrode. For a series of polymers and different injecting electrodes, we find that the current is reduced by one order of magnitude when the injection barrier is increased by only 0.25 eV.[14] We attribute our results to the formation of an increased injection barrier for holes, which suppresses charge injection at the source electrode in these EGOFET devices. This is also corroborated by capacitance–voltage measurements of the metal-insulator-semiconductor structure (MIS) showing a reduced charge carrier density when the transistor is gated with a low work function metal (see Supporting Information, Figure S1). These drain current characteristics are surprising because both the metal-semiconductor and the polyelectrolyte-semiconductor interfaces are identical for all these devices and a lowering of the gate work function is not expected to influence the source–semiconductor interface energetics.

In order to provide a quantitative analysis of the contact resistance (R_C), we extract R_C from the length dependence of the total device resistance, $R_{on} = \partial V_{ds}/\partial I_{ds}$, as ($V_g - V_{th}$) is ranging from 0 to –1.0 V, for a set of devices with L = 50, 20, 10, 8, and 5 μm (i.e., the transmission line method, TLM). In the linear operating regime of the transistor, the channel resistance varies linearly with the channel length. Accordingly, R_C can be extracted for each applied ($V_g - V_{th}$) by determining the y-axis intercept of the data linear fitting (extrapolation to zero channel length).[15] The characteristic R_C versus the gate electrode work function behavior was also confirmed by analyzing the response of similar transistors in a gated four-probe configuration (gFP, see Experimental Section for further details). In both cases we only consider the characteristics of EGOFETs working in the linear regime, that is, where the charge distribution is uniform along the channel. **Figure 2** displays the extracted width-normalized total contact resistance ($R_C W$) versus the gate voltage for different gate metal electrodes. We observe a typical drop of contact resistance with increasing gate voltage, which is commonly observed in staggered device configurations and is due to the combined effect of current crowding[16] and gate-bias assisted charge injection.[17] The difference in the output characteristics of the transistors, as demonstrated in Figure 1c, is well supported by the contact resistance measurements. Indeed, including aluminum as the gate electrode increases the contact resistance of the channel up to nearly one order of magnitude as compared to utilizing Ni. This is consistent with the formation of an increased injection barrier for holes at the source electrode in the EGOFET devices. At sufficiently high gate voltages ($|V_g - V_{th}| > 0.5$ V), where the extraction of contact resistance is more accurate, the gFP measurements (Figure 2b) confirm our aforementioned observation that the Ni gate yields a significantly lower contact resistance for hole injection as compared to the Al gate. It is noteworthy that even in the case of less resistive devices (i.e., Ni gate), the contact resistance is at least three orders of magnitude higher than what typically is reported for similar devices using ionic liquids as the gate dielectric (≈10 Ωcm).[18] This

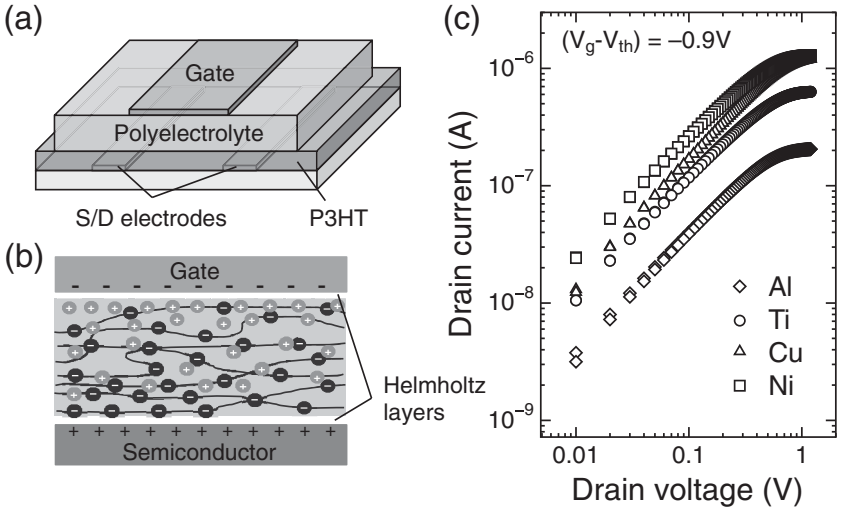

Figure 1. a) Schematic diagram of the polyelectrolyte-gated OFET structure and b) illustration of the channel charge and ion distribution within the polyelectrolyte layer. c) Log–log plot of the output characteristics at a fixed ($V_g - V_{th}$) = –0.9 V for P3HT-based EGOFETs with various gate metals (L = 50 μm and W = 1000 μm).

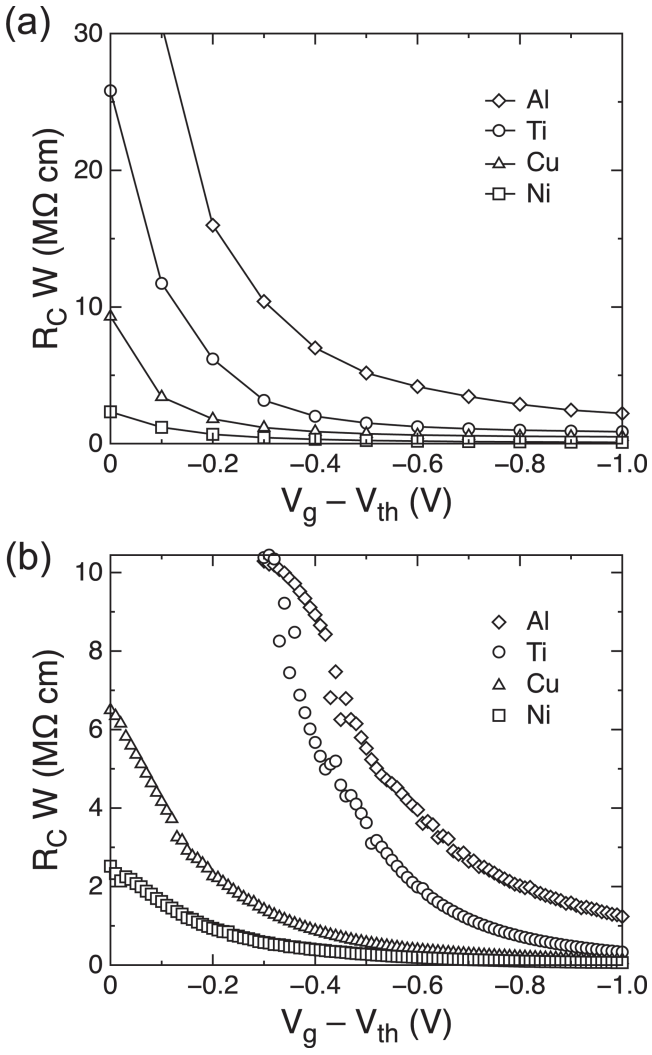

Figure 2. Width-normalized total contact resistance as a function of gate bias for P3HT-based EGOFETs with various gate metals as extracted by a) transmission line method and b) gated four-probe measurement.

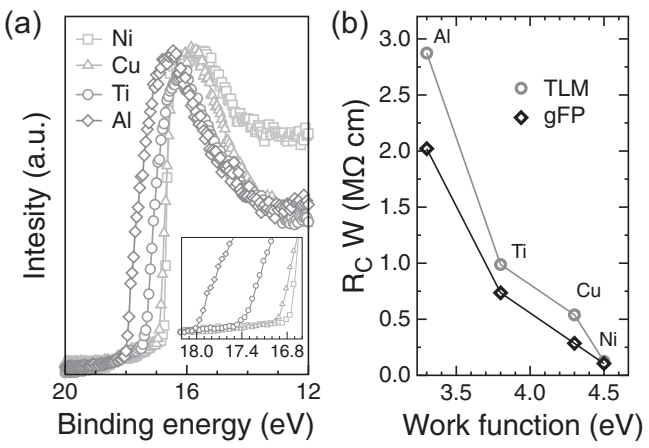

Figure 3. a) Secondary electron cutoff (SECO) spectra showing the evolution of the actual gate metal work function at the polyelectrolyte/gate interface for different gate metals. The inset shows a magnification of the onsets at higher binding energy. b) Width-normalized contact resistance extracted by TLM (circle) and gFP (diamond) methods at $(V_g - V_{th}) = -0.8$ V as a function of the actual gate metal work function.

is because in ionic liquid-gated transistors, and which is also the case for light-emitting electrochemical cells, the injection of holes (or electrons) is assisted by electrostatic screening due to anions (or cations) close to the metal-semiconductor interface, which decreases the width of the Schottky barrier resulting in carrier injection from the source contact via tunneling.[19]

To assess the impact of the gate metal work function on the measured contact resistance, ultraviolet photoemission spectroscopy (UPS) was used to investigate the polyelectrolyte/gate metal interface. In a top-gate OFET geometry the insulator layer is buried under the gate electrode. We take use of an adhesive tape to strip the polyelectrolyte/gate system away from the underlying surface, yielding a gate insulator fully exposed to the ambient, thus making the interface accessible for UPS characterization. Specifically, P(VPA-AA) was spin coated onto a weakly adhering surface such as a planar gold substrate; the gate electrodes were then evaporated on top of the polyelectrolyte layer. The easy exfoliation is due to the low interfacial energy between Au and the P(VPA-AA) layer, which then allows the polyelectrolyte/gate layer to be reliably delaminated. The work function of the different gate metals, as extracted by the secondary electron cutoff (SECO) spectra, is presented in **Figure 3**a and summarized in Table S1 of the Supporting Information. A ≈0.2 eV drop of potential over the polyelectrolyte film (i.e., the difference between peeled and reversed samples) is observed and is most likely due to ordering effects within the polyelectrolyte and not due to any chemical reactions with the gate metal.[20] The variation of the contact resistances is correlated with the measured work function and is reported in Figure 3b. The total contact resistance drops by more than one order of magnitude with systematically increasing the gate work function.

In an attempt to explain the evolution of the contact resistance with the gate metal work function, we proposed the mechanism illustrated in **Figure 4**. When Al is exposed to air (note that polyelectrolyte-gated OFETs operate in ambient condition), a thin native oxide layer is rapidly formed thus lowering the work function up to $\Phi_{AlOx} = 3.5$ eV. Hence, for Al (and Ti), the polyelectrolyte/gate work function is lower than 4.1 eV. First, the difference in Fermi levels between the gate and source electrodes leads to a built-in electric field within the polyelectrolyte, which rearranges the ions distribution. Thus, two Helmholtz double layers are formed at the semiconductor/electrolyte and gate/electrolyte interfaces; negatively charged polyanions are immobile at the Al gate surface (i.e., protons moving away from the surface given the polyelectrolyte used) and protons accumulate at the P3HT/polyelectrolyte interface. Since the electron injection barrier between Au and P3HT is large, a negatively charged channel cannot be formed at the P3HT/polyelectrolyte interface. The negative charges stay at the Au surface and a linear potential drop occurs over the P3HT bulk. Thus, it is expected that a built-in potential is established across the P3HT layer, see Figure 4a. However, because of the weak intermolecular interactions (Van der Waals and π–π interactions) within

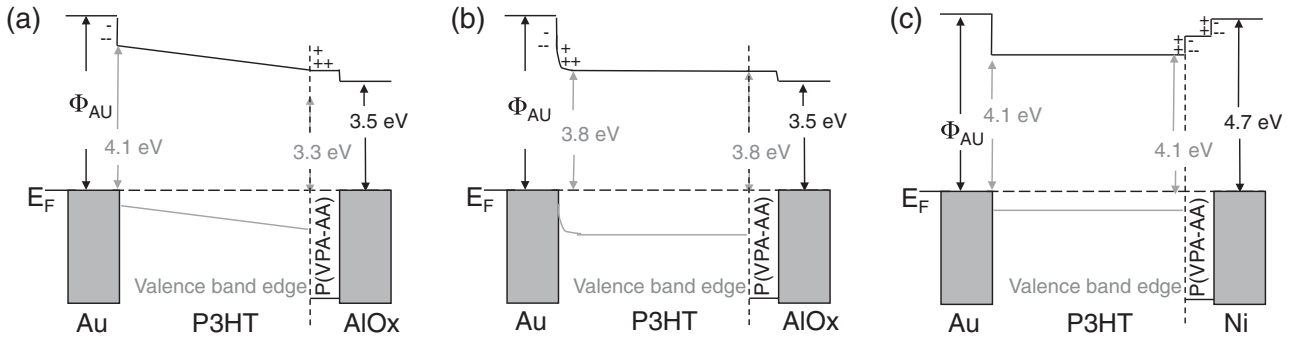

Figure 4. Energy level diagrams of the metal-insulator-semiconductor (MIS) structure showing the effect of the gate metal work function on the energetic of the Au/P3HT interface: a) initial potential profiles as determined by contact work functions and P3HT E_{ICT+}[21] prior to proton migration and b) equilibrium potential profile after proton migration to Au/P3HT contact for Al gate metal comprising a native oxide layer (Φ_{AlOx} = 3.5 eV). c) Equilibrium potential profile as determined by contact work functions and P3HT E_{ICT+} for Ni gate metal.

the P3HT material, protons can penetrate into the semiconductor and are expected to migrate towards the negative charges at the Au contact. This induces a sharp bending of the energy levels inside P3HT in the vicinity of the Au contact (Figure 4b). This bending downshifts the vacuum level and results in an increase of hole-injection barrier at the Au contact, which can explain the high contact resistance with Al gate.

When the modified polyelectrolyte/gate WF is larger than 4.1 eV (as for Ni and Cu), pinning at the P3HT/polyelectrolyte interface according to the so-called positive integer charge transfer state energy,[21] E_{ICT+}, of the P3HT (4.1 eV) is expected to occur (Figure 4c).[22] Holes are then injected from the Au contact and migrate towards the polyelectrolyte interface to cause P3HT slightly *p*-doped and balanced by the negative ion groups of the polyanion (protons then move away from the interface into the polyelectrolyte bulk). At the polyelectrolyte/Ni interface, protons migrate towards the gate contact to balance the negatively charged Ni surface. Hence, most of the potential drop occurs at the P3HT/polyelectrolyte interface. This results in a flat band condition within the P3HT film, with a pinned hole injecting contact at the Au interface and a slightly *p*-doped P3HT region right under the gate contact/polyelectrolyte (≈monolayer). Hence, a near optimal situation. We note that this case is of particular interest for OFETs fabrication since it also applies to high work function metals such as gold (Φ_{Au} = 4.6–4.8 eV), which is typically used as both gate and source/drain electrodes.

Doping can affect the physics of charge injection into the organic semiconductor since it strongly alters the band alignment between the metal and the organic semiconductor. This effect can be significant even at moderate doping levels.[23] This has been extensively investigated for P3HT using several different spectroscopic methods (e.g., ultraviolet/X-ray photoemission spectroscopy) and shows that band alignment at the contact can be drastically affected by doping/dedoping processes, for instance by sequentially exposing the P3HT films to air and vacuum, respectively.[7] Indeed, upon increased doping level the Fermi level in the P3HT will move closer to the HOMO level, resulting in a decrease in the injection barrier by about 0.5 eV.[7] In order to validate our hypothesis that a built-in potential generated by the use of low WF gate metal, such as Al, determines the Fermi-level pinning at the P3HT-Au interface, we exposed the Al-gate-based EGOFETs for several days to ambient atmosphere and then re-measured the electrical characteristics. Our results for doped P3HT EGOFETs quantitatively resemble those obtained for Ni-gated devices, with a contact resistance being 2–3 times lower and a current level of around one order of magnitude higher as compared to what is measured for the pristine Al-gated EGOFETs (**Figure 5**). The same current increase effect is not observed for Ni-gated devices, which agrees with the proposed mechanism.

3. Conclusions

We have found that it is possible to improve the charge injection characteristics in staggered polyelectrolyte-gated OFETs by appropriately choosing the top-gate electrode. The use of low

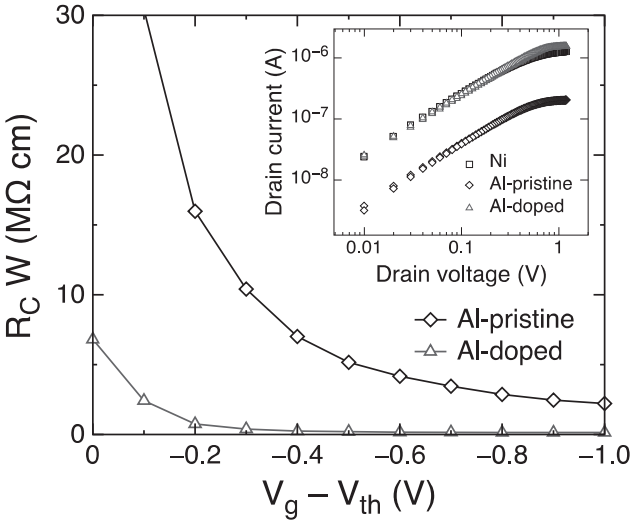

Figure 5. Width-normalized total contact resistance as a function of gate bias for P3HT-based EGOFETs with Al gate metal extracted by transmission line method. The inset shows that I_{ds} increases by almost one order of magnitude upon doping in ambient condition, reaching the same current observed for Ni-gated EGOFETs. The output characteristic of Ni-gated OFET at ($V_g - V_{th}$) = –0.9 V is included for comparison.

work function gate metals (e.g., Al) is found to be detrimental for charge injection at the source electrode, leading to significant Schottky barrier formation for holes at the interface. The contact resistance can be lowered by more than one order of magnitude by using high work function metals such as Ni. We attribute these findings to the establishment of a built-in potential high enough to prevent the Fermi-level pinning at the metal-organic interface, which results in unfavorable energetic alignment of the source electrode with the valence band of the organic semiconductor. It is worthy to stress that precise tuning of the injection characteristics at the source electrode is possible since the operating voltage in the EGOFET devices is comparable to the respective variation of the work functions of the gate electrodes. The possibility to control the charge injection by changing the gate electrode is typically not feasible with conventional inorganic or polymeric dielectric gate insulators since the gate and drain-source driving voltages are relatively much higher. Furthermore, the nature of the polyelectrolyte itself (e.g., dimension and hydrophobicity of the counter ions) could be used as an additional parameter to dictate the charge injection characteristics at the source electrode. This supports the suitability of solid polyelectrolytes as dielectric layers in low voltage-operating devices optimized for circuit applications.

4. Experimental Section

Materials: Regioregular poly(3-hexylthiophene) (P3HT) was purchased from Sigma-Aldrich and used without further purification. The semiconductor was dissolved in 1,2-dichlorobenzene (10 mg mL^{-1}) and filtered with a 0.2 µm polytetrafluoroethylene syringe filter. Poly(vinylphosphonic acid-co-acrylic acid) (P(VPA-AA)) was supplied by Rhodia, dissolved in a mixture of 1-propanol and deionized water (40 mg mL^{-1}) with a solvent ratio of 4:1 and filtered with a 0.2 µm nylon syringe filter.

Device Fabrication: Corning glass substrates were cleaned sequentially in deionized water, acetone and isopropanol. Interdigitated source and drain electrode (3-nm-thick Ti and 25-nm-thick Au) were defined by photolithography and wet etching procedure. The substrates were cleaned carefully again using deionized water, acetone and isopropanol before use. For the transmission line method (TLM), the contact resistance (R_C) was extracted from the length dependence of the total device channel resistance, $R_{on} = \partial V_{ds}/\partial I_{ds}$, as ($V_g - V_{th}$) is ranging from 0 to –1.0 V, for a set of devices with L = 50, 20, 10, 8, and 5 µm. The threshold voltage (V_{th}) was extracted from the transfer curves plotted in a linear scale following the extrapolation in linear region (ELR) method.[13] V_{th} was obtained by adding $V_{ds}/2$ to the intersect with the x-axis. Gated four-probe measurements were performed instead in devices with two narrow voltage probes (2 µm), slightly extending into the channel and being located each at one third of the total channel length (L = 100 µm). The semiconductor layer was formed by spin-coating the warm solution at 2000 rpm for 30 s giving a film thickness of 30 nm. The films were then annealed at 120 °C for 30 min under nitrogen. The polyelectrolyte solution was spin-coated at 2000 rpm for 60 s and dried on a hot plate under vacuum at 120 °C for 120 s, resulting in a thickness of about 130 nm. An 80-nm-thick top electrode for the capacitors and gate electrode for the transistors are formed by thermal evaporation of various metals through a Ni shadow mask (Tecan Ltd.).

Device Characterization: The electrical characteristics of the transistors were measured using a semiconductor parameter analyzer (Keithley 4200-SCS). The impedance measurements were carried out with an Alpha high-resolution dielectric analyzer (Novocontrol GmbH). An AC voltage of 0.001 V was applied, the frequency was set at 1 kHz, and the DC voltage was swept from positive to negative voltages. An equivalent circuit model made of a resistor and a capacitor in parallel was used to extract the effective capacitance, which was calculated from the equation $C = 1/(2\pi f Im(Z))$, where f is the frequency and Z is the measured impedance.

Characterization of Metal/Polyelectrolyte Interfaces: Layers of polyelectrolyte were prepared by spin-coating onto gold substrates sequentially cleaned in deionized water, acetone and isopropanol. The metal top layers were then evaporated in the same manner as for the device preparation. The peel-off procedure was applied with a double-sided copper adhesive tape. Flipping of the double layer samples enabled characterization of the polyelectrolyte side of the polyelectrolyte/metal interface. For determination of the work function ultraviolet photoelectron spectroscopy (UPS) measurements were performed using monochromatized HeI radiation ($h\nu$ = 21.2 eV) in a spectrometer of our own design and construction with resolution of 0.1 eV.

Supporting Information

Supporting Information is available from the Wiley Online Library or from the author.

Acknowledgements

This research is supported by the Advanced Functional Materials Center at Linköping University and the Önnesjö Foundation. Authors wish to thank also the Knut and Alice Wallenberg Foundation (Power Paper project, scholars), VINNOVA, and STEM, the Swedish Energy Agency for financial support.

Received: June 17, 2013
Revised: July 10, 2013
Published online: August 28, 2013

[1] H. Klauk, *Chem. Soc. Rev.* **2010**, *39*, 2643.
[2] a) A. C. Arias, J. D. MacKenzie, I. McCulloch, J. Rivnay, A. Salleo, *Chem. Rev.* **2010**, *110*, 3; b) T. Sekitani, T. Someya, *Adv. Mater.* **2010**, *22*, 2228.
[3] a) D. Natali, M. Caironi, *Adv. Mater.* **2012**, *24*, 1357; b) S. Fabiano, H. Wang, C. Piliego, C. Jaye, D. A. Fischer, Z. H. Chen, B. Pignataro, A. Facchetti, Y. L. Loo, M. A. Loi, *Adv. Funct. Mater.* **2011**, *21*, 4479.
[4] a) Y. L. Shen, A. R. Hosseini, M. H. Wong, G. G. Malliaras, *ChemPhysChem* **2004**, *5*, 16; b) J. H. Li, J. S. Huang, Y. Yang, *Appl. Phys. Lett.* **2007**, *90*, 3.
[5] a) H. Ishii, K. Sugiyama, E. Ito, K. Seki, *Adv. Mater.* **1999**, *11*, 605; b) S. Duhm, G. Heimel, I. Salzmann, H. Glowatzki, R. L. Johnson, A. Vollmer, J. P. Rabe, N. Koch, *Nature Mater.* **2008**, *7*, 326; c) S. Fabiano, H. Yoshida, Z. Chen, A. Facchetti, M. A. Loi, *ACS Appl. Mater. Interfaces* **2013**, *5*, 4417.
[6] a) D. B. A. Rep, A. F. Morpurgo, T. M. Klapwijk, *Org. Electron.* **2003**, *4*, 201; b) Y. Zhang, P. W. M. Blom, *Appl. Phys. Lett.* **2010**, *97*, 083303.
[7] B. H. Hamadani, H. Ding, Y. Gao, D. Natelson, *Phys. Rev. B* **2005**, *72*, 235302.
[8] N. Koch, S. Duhm, J. P. Rabe, A. Vollmer, R. L. Johnson, *Phys. Rev. Lett.* **2005**, *95*, 237601.
[9] B. H. Hamadani, D. A. Corley, J. W. Ciszek, J. M. Tour, D. Natelson, *Nano Lett.* **2006**, *6*, 1303.
[10] X. Cheng, Y.-Y. Noh, J. Wang, M. Tello, J. Frisch, R.-P. Blum, A. Vollmer, J. P. Rabe, N. Koch, H. Sirringhaus, *Adv. Funct. Mater.* **2009**, *19*, 2407.

[11] L. Herlogsson, X. Crispin, N. D. Robinson, M. Sandberg, O. J. Hagel, G. Gustafsson, M. Berggren, *Adv. Mater.* **2007**, *19*, 97.
[12] L. Herlogsson, Y. Y. Noh, N. Zhao, X. Crispin, H. Sirringhaus, M. Berggren, *Adv. Mater.* **2008**, *20*, 4708.
[13] L. Kergoat, L. Herlogsson, B. Piro, P. Minh Chau, G. Horowitz, X. Crispin, M. Berggren, *Proc. Natl. Acad. Sci. U. S. A.* **2012**, *109*, 8394.
[14] K. Asadi, T. G. de Boer, P. W. M. Blom, D. M. de Leeuw, *Adv. Funct. Mater.* **2009**, *19*, 3173.
[15] B. H. Hamadani, D. Natelson, *Appl. Phys. Lett.* **2004**, *84*, 443.
[16] T. J. Richards, H. Sirringhaus, *J. Appl. Phys.* **2007**, *102*, 094510.
[17] J. J. Brondijk, F. Torricelli, E. C. P. Smits, P. W. M. Blom, D. M. de Leeuw, *Org. Electron.* **2012**, *13*, 1526.
[18] D. Braga, M. J. Ha, W. Xie, C. D. Frisbie, *Appl. Phys. Lett.* **2010**, *97*, 193311.
[19] J. C. de Mello, N. Tessler, S. C. Graham, R. H. Friend, *Phys. Rev. B* **1998**, *57*, 12951.
[20] W. Osikowicz, M. P. de Jong, S. Braun, C. Tengstedt, M. Fahlman, W. R. Salaneck, *Appl. Phys. Lett.* **2006**, *88*, 193504.
[21] a) S. Braun, W. R. Salaneck, M. Fahlman, *Adv. Mater.* **2009**, *21*, 1450; b) S. Braun, X. Liu, W. R. Salaneck, M. Fahlman, *Org. Electron.* **2010**, *11*, 212; c) G. Brocks, D. Cakir, M. Bokdam, M. P. de Jong, M. Fahlman, *Org. Electron.* **2012**, *13*, 1793.
[22] Here we assume again that the ≈0.2 eV potential drop over the polyelectrolyte film (peeled and reversed samples) is due to ordering effects in the polyelectrolyte and are not due to chemical reactions with the gate metal, although this would make only minor difference as discussed for the P3HT case (see Ref. 20. Due to the polyelectrolyte we expect that half of the necessary potential drop occurs at the P3HT/polyelectrolyte interface (4.65–4.1 = 0.55 eV; half 0.275 eV).
[23] G. Lu, J. Blakesley, S. Himmelberger, P. Pingel, J. Frisch, I. Lieberwirth, I. Salzmann, M. Oehzelt, R. Di Pietro, A. Salleo, N. Koch, D. Neher, *Nat. Commun.* **2013**, *4*, 1588.